Journal of Magnetic Resonance 208 (2011) 103–113

Contents lists available at ScienceDirect

Journal of Magnetic Resonance

journal homepage: www.elsevier.com/locate/jmr

New methods for the acquisition of ultra-wideline solid-state NMR spectra of spin-1/2 nuclides

Alan W. MacGregor, Luke A. O'Dell, Robert W. Schurko *

Department of Chemistry and Biochemistry, University of Windsor, Windsor, Ontario, Canada N9B 3P4

ARTICLE INFO

Article history:
Received 8 July 2010
Revised 15 October 2010
Available online 28 October 2010

Keywords:
Solid-state NMR
^{119}Sn
^{195}Pt
^{199}Hg
^{207}Pb
WURST–CPMG
Optimal control theory

ABSTRACT

The Wideband Uniform Rate Smooth Truncation – Carr–Purcell Meiboom–Gill (WURST–CPMG) pulse sequence was recently introduced as a new method of acquiring ultra-wideline solid-state NMR (SSNMR) patterns of quadrupolar nuclei (Chem. Phys. Lett. 464 (2008) 97). Herein, we describe the application of the WURST–CPMG pulse sequence to stationary samples (*i.e.,* non-spinning or "static" samples) of various spin-1/2 nuclides (^{119}Sn, ^{207}Pb, ^{199}Hg and ^{195}Pt) in order to examine its effectiveness for acquiring ultra-wideline SSNMR patterns. WURST–CPMG is compared to the CPMG and Cross Polarization (CP)–CPMG pulse sequences in select cases (^{119}Sn and ^{207}Pb, respectively), and its usefulness in obtaining ultra-wideline SSNMR spectra in a piecewise fashion is explored. In addition, a preliminary investigation of pulses generated using optimal control theory (OCT) for the purpose of wideline excitation is presented; spectra acquired using these pulses are compared with standard, rectangular pulses of similar pulse powers. Both methods show much promise for acquiring high quality wideline patterns dominated by chemical shift anisotropy, with minimal distortions and significantly reduced experimental times.

1. Introduction

Solid-state NMR (SSNMR) powder patterns can vary in breadth from a few Hz to several MHz. In the former extreme, the widths of the spectral lines are on the order of those encountered in many solution-state NMR spectra. Such narrow lines occur in SSNMR spectra due to the absence of large anisotropic interactions or dipolar couplings, low magnetic susceptibility broadening, averaging via mechanical rotation and/or specialized pulse sequences, or combinations of these factors. However, the latter extreme describes the situation for many nuclides across the periodic table, where large anisotropic interactions dominate the appearance of the NMR powder patterns, and techniques for averaging (or partially averaging) these interactions are generally ineffective. Nonetheless, there is much information to be garnered from the acquisition of such patterns; in particular, analysis of the anisotropic NMR interaction tensors which give rise to these broad patterns can provide detailed information on structure and dynamics at the molecular level.

Wideline NMR spectroscopy is a term that has been in use since the 1950's to refer to NMR experiments conducted on nuclei with broad patterns arising from anisotropic dipole–dipole interactions (*e.g.,* ^{1}H, ^{19}F), quadrupolar interactions (*e.g.,* ^{2}H) and large chemical shift anisotropies (*e.g.,* ^{207}Pb, ^{199}Hg, etc.). Typically, these patterns range in breadth from tens of kHz to *ca.* 300 kHz. However, there are numerous nuclei, both spin-1/2 and quadrupolar (*i.e.,* spin >1/2), which can yield NMR patterns with breadths of hundreds of kHz to tens of MHz. Acquisition of such NMR spectra can be challenging, since (i) the signal intensity is spread over a wide spectral range, thereby decreasing the inherent signal-to-noise ratio (S/N), (ii) standard, high-power rectangular pulses are insufficient for uniform excitation of these broad patterns [1] and (iii) the probe detection bandwidths are often very limited. Such spectra require specialized methodologies, pulse sequences and/or hardware. We have previously suggested the term *ultra-wideline* (UW) *NMR spectroscopy* to describe the set of techniques designed to ensure uniform excitation of such extremely broad patterns [2]. Improvements in NMR hardware, the availability of ultra-high field NMR spectrometers and the introduction of an array of different pulse sequences and experimental schemes have made the acquisition of UW NMR spectra feasible, and opened up the periodic table of NMR-active nuclides to investigation via SSNMR [3–9].

Early UW NMR spectra were acquired using a "point-by-point" method, where the transmitter is stepped in even increments across the entire spectral range at constant magnetic field, and the echo intensity is plotted as a function of the transmitter frequency to obtain the total powder pattern [10,11]. There are recent reports that feature this acquisition technique, or describe experiments in which the magnetic field is incrementally stepped while

* Corresponding author. Fax: +1 519 973 7098.
E-mail address: rschurko@uwindsor.ca (R.W. Schurko).
URL: http://www.uwindsor.ca/schurkohttp://chemistry.uvic.ca (R.W. Schurko).

1090-7807/$ - see front matter © 2010 Elsevier Inc. All rights reserved.
doi:10.1016/j.jmr.2010.10.011

holding the transmitter frequency constant [3,12]. This basic technique is very time-consuming, since a large number of experiments must be conducted to obtain an UW NMR spectrum of reasonable resolution. However, it was later suggested that the total UW NMR experiment can be conducted more efficiently by acquiring echoes at evenly spaced transmitter offsets, Fourier transforming the individual echoes, and then coadding [13,14] or skyline projecting [15] the resulting sub-spectra to produce the final pattern. This reduces the number of experiments required to obtain the complete powder pattern, and provides spectral resolution more closely associated with the dwell time of the echo experiment than the transmitter spacing.

There have been several modifications to the aforementioned UW NMR techniques that involve specialized pulse sequences or hardware. The quadrupolar Carr–Purcell Meiboom–Gill (QCPMG) pulse sequence, which was reintroduced for the acquisition of wideline NMR spectra of half-integer quadrupolar nuclei [16], has been particularly useful in enhancing the S/N of individual sub-spectra and reducing total acquisition times in UW NMR experiments [15,17–22]. Another recently explored method for acquiring UW NMR spectra involves the use of microcoils [2,23,24], which typically have a 1.5 mm inner diameter or less. Microcoils are capable of producing large, homogeneous B_1 fields from very modest power inputs. This feature partially offsets the loss in S/N from reduced sample size and allows for excitation pulses with correspondingly wider excitation bandwidths. In addition, the small coil size may be advantageous in cases where only a limited amount of sample is available.

A recent development in the acquisition of UW spectra was initiated by Bhattacharyya and Frydman [25], who proposed the use of Wideband Uniform Rate Smooth Truncation (WURST) broadband excitation pulses [26], which greatly increase excitation bandwidths without the need for specialized hardware. Our group has recently expanded upon this work with the WURST–QCPMG pulse sequence [22], which utilizes a train of WURST pulses and acquisition windows in a fashion similar to the QCPMG sequence. The combination of the broad excitation bandwidths of WURST pulses with the signal enhancements of the QCPMG sequence has proven useful in the acquisition of NMR spectra of both half-integer and integer quadrupolar nuclei [27].

Another potential method for acquiring UW NMR spectra lies in using optimal control theory (OCT), which was recently implemented in the SIMPSON (ver. 2.0) software package [28,29]. OCT can be used to numerically optimize a system composed of a very large number of variables, and can therefore be utilized to adjust RF amplitude and phase modulations in order to obtain an "optimal NMR pulse sequence" in which the experimental efficiency is maximized. OCT has been used to generate broadband excitation schemes for high-resolution ^{13}C NMR at high fields, with excitation profiles of approximately 50 kHz [30–32], as well as for half-integer quadrupolar nuclei [33]. However, to the best of our knowledge, OCT has not yet been employed to optimize broadband excitation pulses for the acquisition of static UW powder patterns.

UW NMR studies to date have largely focussed on half-integer quadrupolar nuclei with broad central-transition NMR spectra resulting from large nuclear quadrupole moments and/or low gyromagnetic ratios coupled with sizeable electric field gradients (EFGs) [8,9,15,19,34–36]. However, there are several heavy spin-1/2 nuclei such as ^{119}Sn, ^{195}Pt, ^{199}Hg and ^{207}Pb, which often have large chemical shift anisotropies (CSAs) and correspondingly broad patterns that could potentially be acquired efficiently using UW NMR experiments. For instance, Slichter and co-workers published several papers in the 1980's on ^{195}Pt NMR of catalytic platinum nanoparticles adsorbed on alumina, where the stepwise method was used to acquire ^{195}Pt NMR spectra up to *ca.* 4 MHz in breadth [10,37]. Ellis and coworkers also carried out UW ^{195}Pt NMR experiments, though they employed MAS to acquire the extremely broad spectrum of K_2PtCl_4 [38]. MAS techniques have also been used to acquire broad ^{119}Sn [39,40] and ^{199}Hg spectra [41]. However, we note that in two recent papers on UW ^{207}Pb and ^{195}Pt SSNMR [42,43] that MAS experiments on nuclei with extremely broad patterns are often unreliable, due to slight mis-sets of the magic-angle [44] and/or incomplete excitation of the manifold of spinning sidebands, both of which yield patterns which do not allow for accurate assessments of the chemical shift tensor parameters.

In 2004, our research group, and Siegel et al., examined the effectiveness of the CPMG pulse sequence in acquiring the NMR spectra of various spin-1/2 nuclei [45,46]. These experiments are especially useful when cross-polarization (CP)/MAS NMR experiments are limited by weak dipolar couplings and poor excitation bandwidths, or other complications arising from acquisition of broad powder patterns using MAS NMR [44,47,48]. ^{1}H–X (where X is a heavy spin-1/2 nucleus) CP–CPMG experiments are capable of yielding high quality UW NMR spectra from which chemical shift tensors can be readily extracted; however, the acquisitions of broad patterns are labour intensive, requiring the collection of many sub-spectra due to the limited excitation bandwidth associated with CP [42]. CPMG can also be used to directly excite the X nuclei with modest improvements in excitation bandwidth with respect to the CP–CPMG experiments; however, such experiments still require numerous sub-spectra to be acquired and are often hampered by large longitudinal (T_1) relaxation time constants.

Herein, we improve upon the efficiency of previous UW NMR experiments on heavy spin-1/2 nuclides via application of the WURST–CPMG pulse sequence (WURST–CPMG is the exact same sequence as WURST–QCPMG, but since this paper does not deal with quadrupolar nuclei, we have omitted the "Q" as it does not apply here). UW ^{119}Sn, ^{207}Pb, ^{199}Hg and ^{195}Pt NMR spectra are acquired for some samples with large chemical shift anisotropies, and compared to data from analogous CPMG and CP–CPMG experiments, as appropriate. In addition, we also present the first attempt at utilizing pulses designed using OCT for uniform excitation of CSA-dominated powder patterns.

2. Results and discussion

2.1. WURST–CPMG SSNMR experiments

2.1.1. ^{119}Sn NMR

Tin has three NMR-active isotopes, ^{115}Sn, ^{117}Sn and ^{119}Sn; however, ^{119}Sn is generally chosen for tin NMR studies as it has the highest natural abundance (8.58%) and highest gyromagnetic ratio (-9.99760×10^7 rad T^{-1} s^{-1}, corresponding to 149.29 MHz at 9.4 T). Solid-state ^{119}Sn NMR has been used to study a wide variety of systems, including stannates [39,49,50], nanoparticles [51–53], and various organotin materials [54–56], among others. We have chosen SnO as a model system on which to test ^{119}Sn WURST–CPMG because of its high tin content and its large (975 ppm) span [40].

The ^{119}Sn NMR spectra of SnO acquired using the CPMG and WURST–CPMG pulse sequences are depicted in Fig. 1. The powder patterns are *ca.* 160 kHz in breadth, and clearly indicate that the CS tensor is axially symmetric (*vide infra*). The pattern breadth is beyond the excitation bandwidth of standard rectangular pulses applied at commonly attainable RF powers; in this case, the CPMG experiment utilized $\pi/2$ pulses of *ca.* 3.3 μs ($\nu_1 \approx 75$ kHz). The CPMG spectrum (Fig. 1A) was acquired in a piecewise frequency-stepped manner, with 10 sub-spectra (80 transients per subspectrum) to complete the total pattern. The total spectrum was acquired in 27 min, not including the time required to retune the probe for each transmitter frequency. The WURST–CPMG (Fig. 1B) spectrum was acquired in a single, 80 scan

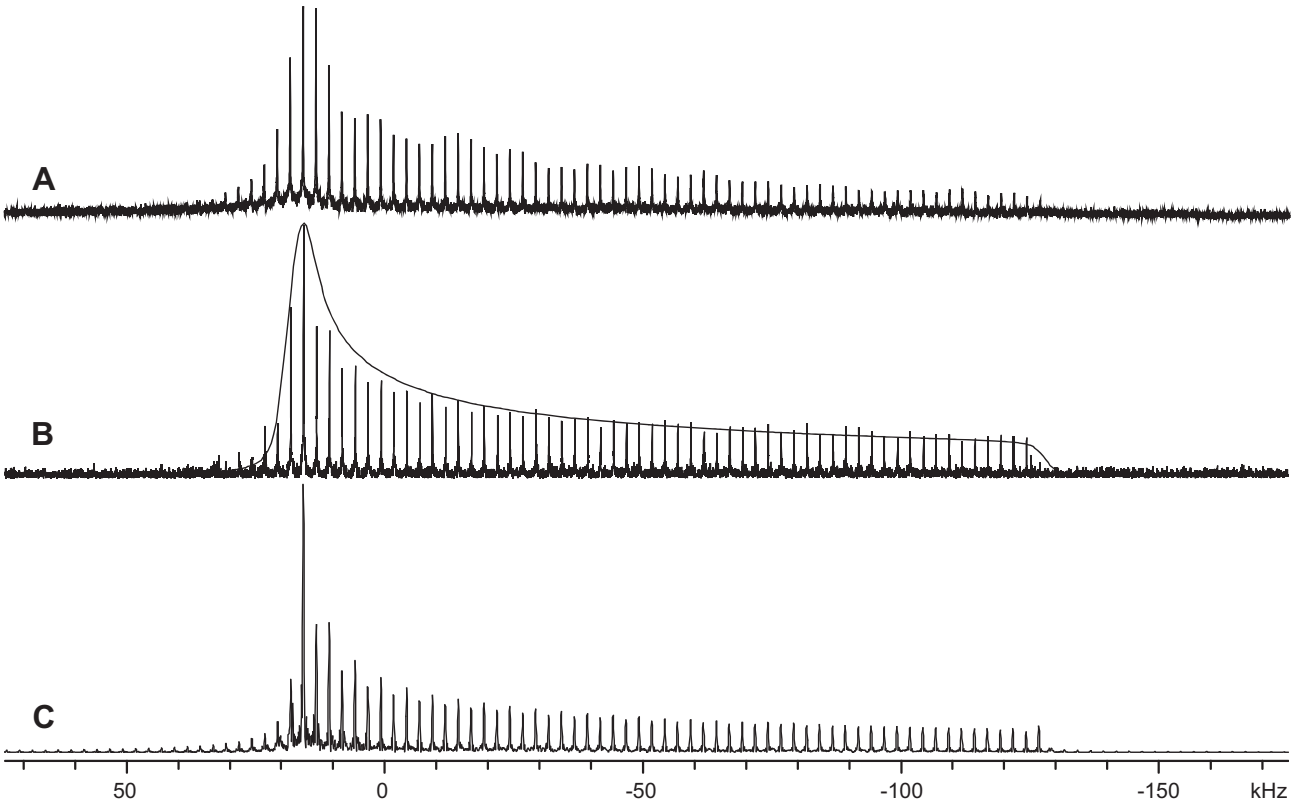

Fig. 1. (A) ^{119}Sn CPMG NMR spectrum of SnO produced from the co-addition of 10 sub-spectra, each of which consists of 80 averaged transients. (B) Bottom trace: ^{119}Sn WURST–CPMG NMR spectrum of SnO. The spectrum consists of 80 averaged transients and was acquired in a single experiment. Top trace: analytical simulation based on the co-addition of the echoes from the WURST–CPMG experiment. (C) SIMPSON simulation of ^{119}Sn WURST–CPMG NMR spectrum of SnO.

experiment which employed pulses with RF fields of 30 kHz and took *ca.* 3 min to complete, a reduction in experimental time of almost an order of magnitude (Table 1). The S/N is comparable in the CPMG and WURST–CPMG spectra; however, there is a pronounced modulation along the breadth of the CPMG spectrum which is not visible in the WURST–CPMG spectrum, arising from the transmitter spacings and short echo delays chosen for this set of experiments. The CS tensor parameters are obtained by fitting a simulated pattern to either the outer manifold of the WURST–CPMG spikelet spectrum, or to a spectrum produced by Fourier transforming an FID constructed from the coaddition of the WURST–CPMG spin-echoes in the time domain. Our simulation indicates that the CS parameters of SnO are $\delta_{iso} = -208(7)$ ppm, $\Omega = 988(25)$ ppm and $\kappa = 1$ (Table 2). These data agree well with the results of Cossement et al., $\delta_{iso} = -208(7)$ ppm, $\Omega = 975(15)$ ppm and $\kappa = 1$ [40]. A SIMPSON simulation of the WURST–CPMG spikelet manifold (Fig. 1C) confirms the accuracy of the simulated parameters.

We note that the comparisons of the experimental data to the simulated powder and CPMG patterns are made solely to obtain estimates for the chemical shift tensor parameters and their uncertainties, the latter of which are estimated by both visual comparison of experimental and simulated data, as well as consideration of the spikelet spacings. Distortions in the experimental spectra that may arise from improper transmitter offsets, finite pulse widths, etc., which are augmented by the inherently low S/N ratios, are not accounted for in the numerically simulated spectra. Fortunately, relatively accurate determination of the chemical shift tensor parameters are not hindered in this case, nor any of the cases below, since their values are dependent solely upon the positions of the three discontinuities.

2.1.2. ^{207}Pb NMR

^{207}Pb NMR experiments can be challenging to carry out because of the vast chemical shift range of lead, as well as the generally large lead chemical shift anisotropies and long T_1 relaxation times

Table 1
Comparison of total experimental times for CPMG, CP–CPMG and WURST–CPMG experiments.

	SnO		$Pb(OAc)_2{\cdot}3H2O$		$Hg(OAc)_2$	K_2PtCl_4
	CPMG	WURST–CPMG	CP–CPMG	WURST–CPMG	WURST–CPMG	WURST–CPMG
Sub-spectra[a]	10	1	9	1	1	5
Scans per subspectrum	80	80	192	248	72	40
Recycle delay (s)	2	2	4	7	1450	40
Step size (kHz)[b]	45	N/A	20	N/A	N/A	400
Experimental time[c] (mins)	26.7	2.7	115.2	28.9	1740	133.3

[a] Denotes the number of sub-spectra required to collect the entire powder pattern with piecewise acquisition. A value of 1 indicates that piecewise acquisition was not required.
[b] Denotes the spacing between transmitter frequencies of sub-spectra in piecewise experiments.
[c] Experimental times listed do not account for the time required to retune the probe and change the transmitter frequency between sub-spectra in piecewise experiments.

Table 2
Comparison of experimental chemical shift parameters with values reported in the literature[a].

Compound	δ_{iso}[b] (ppm)	Ω[c] (ppm)	κ[d]	δ_{11} (ppm)	δ_{22} (ppm)	δ_{33} (ppm)	Ref.[e]
SnO (exp.)	−208 (12)	988 (24)	1[f]	121 (17)	121 (17)	−867 (17)	
SnO (lit.)	−208 (7)	975 (15)	1[f]	117 (9)	117 (9)	−858 (12)	[40]
$Pb(OAc)_2$ (exp.)	−1890 (24)	1690 (48)	0.61 (5)	−1217 (34)	−1546 (34)	−2906 (34)	
$Pb(OAc)_2$ (lit.)	−1881 (7)	1690 (14)	0.65 (2)	−1219 (11)	−1515 (14)	−2909 (12)	[45]
$Pb(OAc)_2$ (lit.)	−1904 (10)	1728 (10)	0.62 (2)	−1219 (12)	−1546 (15)	−2947 (13)	[65]
$Hg(OAc)_2$ (exp.)	−2513 (34)	1810 (68)	0.89 (7)	−1876 (48)	−1976 (48)	−3686 (48)	
$Hg(OAc)_2$ (lit.)	−2497	1826	0.9[g]	−1858	−1949	−3684	[71]
K_2PtCl_4 (exp.)	−1520 (113)	10,410 (226)	−1	5420 (160)	−4990 (160)	−4990 (160)	
K_2PtCl_4 (lit.)	−1848 (35)	10,414 (9)	−1[h]	5095 (36)	−5319 (35)	−5319 (35)	[38]

[a] The chemical shielding of each nucleus is represented as a tensor described by three principal components calculated from values of δ_{iso}, κ, and Ω. These principal components are arranged so that $\delta_{11} \geqslant \delta_{22} \geqslant \delta_{33}$. Uncertainties in the principal components are estimated as $\sqrt{2}$ times the spikelet spacing (in ppm), and uncertainties in δ_{iso}, Ω and κ are obtained by propagation of error.

[b] $\delta_{iso} = (\delta_{11} + \delta_{22} + \delta_{33})/3$. Values are with respect to reference standards given in the experimental section.

[c] $\Omega = (\delta_{11} - \delta_{33})$, based upon simulations of static WURST–CPMG spectra.

[d] $\kappa = 3(\delta_{22} - \delta_{iso})/\Omega$, $-1.0 \leqslant \kappa \leqslant 1.0$.

[e] Indicates the relevant reference for values reported in the literature.

[f] This value is fixed at one due to the axial symmetry at the Sn site in SnO, where the Sn atom sits atop a square pyramid with equal Sn—O bond lengths of 2.225(8) Å (see Ref. [40]).

[g] Uncertainties not reported.

[h] The skew is fixed at −1 due to the D_{4h} symmetry of the $PtCl_4^{2-}$ anion.

[57–61]. However, ^{207}Pb NMR is an extremely sensitive probe of the local Pb environment and has become an important tool in the characterization of lead-containing materials [61]. ^{207}Pb NMR has recently been applied to study technologically advanced materials such as waste disposal media [57] and materials relevant to lead-based superconductors [57,58]. The high sensitivity of the ^{207}Pb chemical shifts to small changes in sample temperature has contributed to the use of various lead-containing samples as "NMR thermometers [62,63]".

For lead-containing samples where protons are present, ^{1}H–^{207}Pb CP/MAS NMR experiments are typically applied, due to the enhancement afforded from CP and the dependence of the experimental recycle time on the T_1 of the protons (as opposed to the T_1 constants of ^{207}Pb, which are usually much longer) [59]. In numerous cases where the CP efficiency is greatly reduced under conditions of MAS (even under slow spinning), static piecewise ^{1}H–^{207}Pb CP–CPMG NMR experiments are useful for the acquisition of ^{207}Pb NMR spectra. However, many ^{207}Pb NMR spectra are far too broad to be obtained in a single experiment, even under conditions of MAS [38,42]. $Pb(OAc)_2{\cdot}3H_2O$ is often used as a setup standard for stationary ^{1}H–^{207}Pb CP–CPMG NMR experiments, due to its relatively narrow pattern and short ^{1}H T_1 (*ca.* 7 s) [45,64,65]. However, the breadth of the ^{207}Pb NMR spectrum of $Pb(OAc)_2{\cdot}3H_2O$ (at 9.4 T) far exceeds the excitation bandwidth of the CP–CPMG sequence, which is dependent upon the Hartmann–Hahn matching condition (which can only be achieved across a relatively narrow range of frequencies). Direct excitation of the nucleus (*i.e.,* without CP), though also limited in bandwidth, has been shown to be more useful for the acquisition of broad NMR patterns [66]. Consequently, we employed WURST–CPMG to attempt an acquisition of the entire powder pattern of $Pb(OAc)_2{\cdot}3H_2O$ in a single experiment.

Fig. 2 depicts the spectra of $Pb(OAc)_2{\cdot}3H_2O$ acquired with CP–CPMG (Fig. 2A) and WURST–CPMG (Fig. 2B). The spectra are *ca.* 138 kHz in breadth, with clearly defined discontinuities. The CSA-dominated powder pattern is too broad to be acquired with a single CP–CPMG experiment, necessitating the use of the piecewise frequency-stepped method. A total of 9 sub-spectra were acquired to construct the complete powder pattern, each of which took just under 13 min to obtain (*ca.* 115 min to acquire the complete pattern, not including the time required to retune the probe, Table 1). The WURST–CPMG ^{207}Pb NMR spectrum of $Pb(OAc)_2{\cdot}3H_2O$ was acquired in a single 248 scan experiment that required just under 30 min to complete. The WURST–CPMG pattern has a much higher S/N ratio and more clearly resolved discontinuities than the CP–CPMG pattern; in addition, the former required no special processing (*i.e.,* coaddition of sub-spectra). Simulation of the spectrum resulting from the time domain coadded echoes of the WURST–CPMG experiment yields $\delta_{iso} = -1890$ ppm, $\Omega = 1690$ ppm and $\kappa = 0.61$, all of which agree very well with previously reported parameters (Table 2) [45,64,65]. A SIMPSON simulation of the ^{207}Pb WURST–CPMG spikelet manifold (Fig. 2C) using these parameters again further confirms the accuracy of these values.

Due to the use of lead acetate as a ^{207}Pb SSNMR setup standard, it is worth noting that our first attempts to acquire these spectra resulted in distorted powder patterns with a pronounced "lump" at the high-frequency end of the pattern (Fig. S1). However, recrystallization of the sample from aqueous solution significantly changed the appearance of the ^{207}Pb UW NMR spectrum, leading us to conclude that the initial sample was partially dehydrated. Indeed, the same phenomenon was acknowledged in our group's previous paper involving lead acetate hydrate, though a more pronounced shift to high-frequency was noted [45].

2.1.3. ^{199}Hg NMR

Mercury has two NMR-active isotopes, ^{199}Hg and ^{201}Hg. The former is preferred for NMR spectroscopy due to its higher natural abundance (16.8%), higher gyromagnetic ratio (4.8458×10^7 rad T^{-1} s^{-1}, $\nu_0 = 72.5$ MHz at 9.4 T) and the fact that it is a spin-1/2 nucleus (^{201}Hg is a spin-3/2 nucleus). ^{199}Hg NMR has been used extensively to probe the atomic environment of metal centres in biologically relevant materials by using ^{199}Hg as a surrogate nucleus for less receptive nuclei (*e.g.,* ^{67}Zn) [67], or to study model compounds of metal centres in proteins [44]. Solid-state ^{199}Hg NMR data have been collected for many different types of mercury-containing compounds, from dimercury (I) species [68] to organometallic molecules [41]. Like ^{207}Pb, ^{199}Hg also has an expansive chemical shift range [69], and many ^{199}Hg SSNMR spectra exhibit large CSAs, making ^{199}Hg SSNMR extremely sensitive to changes in local Hg environments. $Hg(OAc)_2$ was chosen as a test sample for ^{199}Hg WURST–CPMG NMR experiments because of its use as a CP setup standard in ^{199}Hg CP/MAS NMR experiments, as well as its well-characterized CS tensor parameters [45,70].

Fig. 3 shows the ^{199}Hg WURST–CPMG NMR spectrum of $Hg(OAc)_2$. The spectrum is *ca.* 130 kHz broad, and indicates a mercury CS tensor of nearly axial symmetry. 72 scans were used to acquire the ^{199}Hg WURST–CPMG NMR spectrum, resulting in a total experimental time of *ca.* 29 h. A long recycle delay of 1450 s was

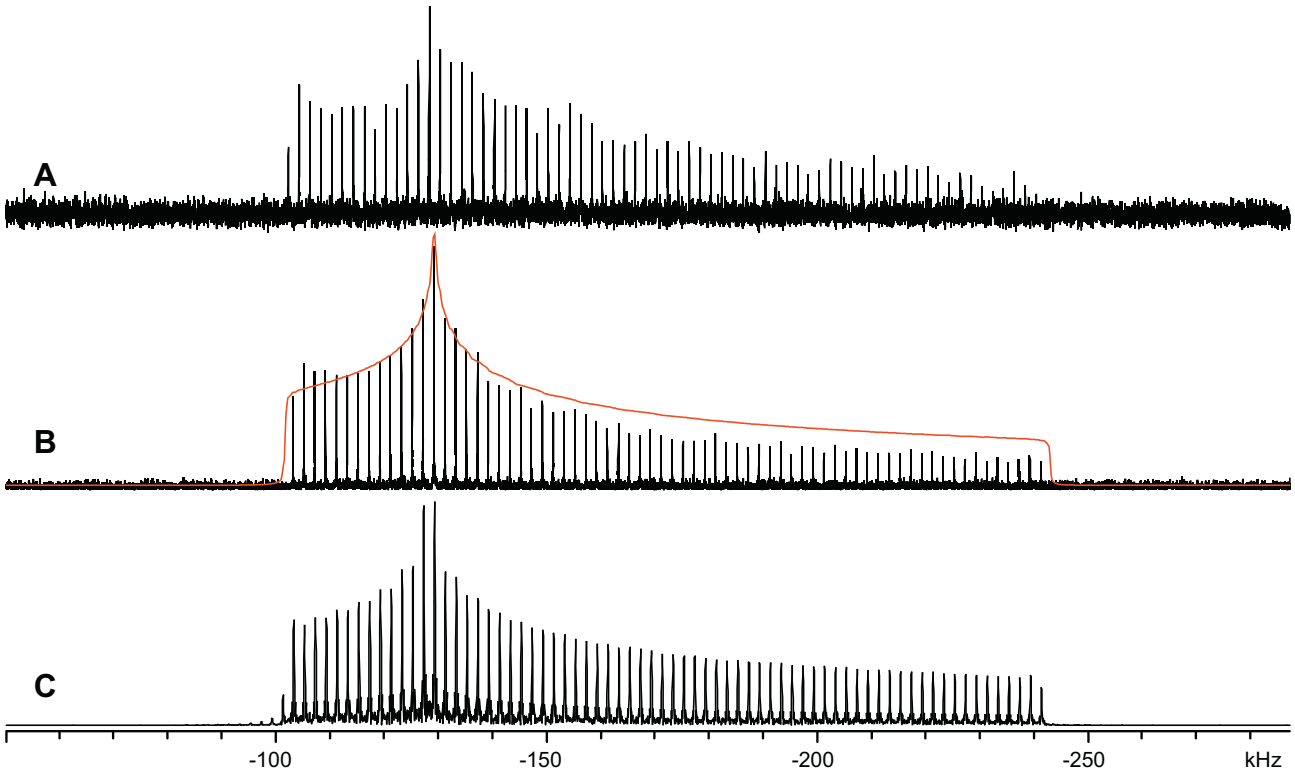

Fig. 2. (A) ^{207}Pb CP–CPMG NMR spectrum of $Pb(OAc)_2{\cdot}3H_2O$ from the co-addition of nine sub-spectra, each of which consists of 192 averaged transients. (B) Bottom trace: ^{207}Pb WURST–CPMG NMR spectrum of $Pb(OAc)_2{\cdot}3H_2O$ from the collection of 248 averaged transients in a single experiment. Top trace: analytical simulation based on the co-addition of the echoes from the WURST–CPMG experiment. (C) SIMPSON simulation of the ^{207}Pb WURST–CPMG NMR spectrum of $Pb(OAc)_2{\cdot}3H_2O$.

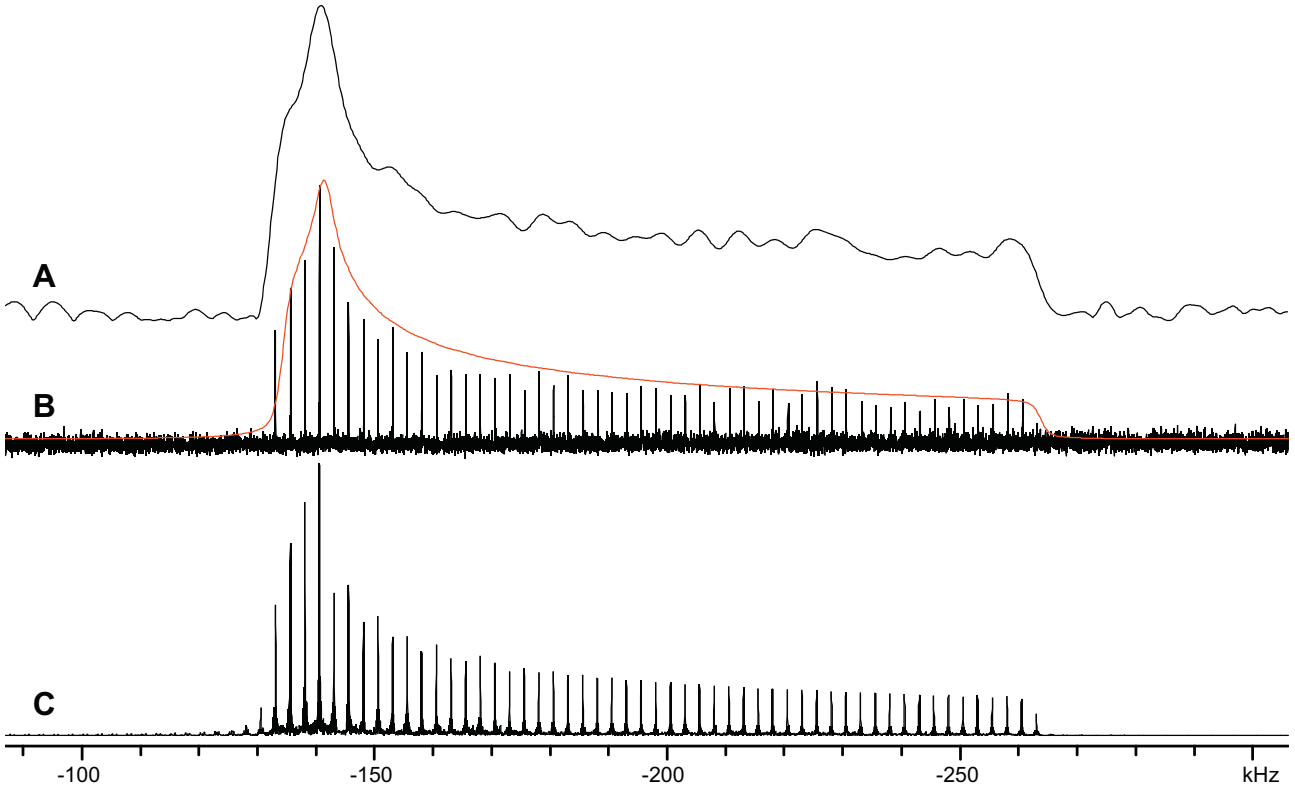

Fig. 3. (A) Echo spectrum resulting from Fourier transformation of the sum of the spin-echoes of the ^{199}Hg WURST–CPMG experiment. (B) Bottom trace: ^{199}Hg WURST–CPMG NMR spectrum of $Hg(OAc)_2$. Top trace: analytical simulation based on the spectrum in A. (C) SIMPSON simulation of the ^{199}Hg WURST–CPMG NMR spectrum of $Hg(OAc)_2$.

applied for this experiment, due to the large $T_1(^{199}Hg)$ relaxation time constants [71]. Our group previously acquired the ^{199}Hg NMR spectrum of $Hg(OAc)_2$ with a piecewise ^1H–^{199}Hg CP–CPMG experiment that required the acquisition of 6 sub-spectra [45], each subspectrum took 16 scans to acquire for the CP–CPMG experiments, and the entire experimental time required was *ca.* 2.4 h (Table 1). Wasylishen et al. also acquired the ^{199}Hg NMR spectrum of $Hg(OAc)_2$ using CP–CPMG, which required the acquisition of 9 sub-spectra and took *ca.* 5 h [46]. The use of WURST–CPMG does not reduce the time required to obtain the ^{199}Hg NMR spectrum of $Hg(OAc)_2$ compared to the CP–CPMG experiment, largely due to the dependence of the recycle delay of the latter on the much shorter proton T_1. However, our experiment demonstrates that the WURST–CPMG sequence can be readily employed to acquire ^{199}Hg NMR spectra in cases where CP is not a viable option (*i.e.*, little or no CP efficiency due to the absence of abundant and/or mobile nuclei, etc.). Again, the other benefit of using WURST–CPMG is that the entire powder pattern may be acquired without stepping the transmitter, and hence, no probe retuning is required. Fitting of the CP–CPMG spectrum with SIMPSON yielded $\delta_{iso} = -2513$ ppm, $\Omega = 1810$ ppm and $\kappa = 0.89$, which match well with previous values ($\delta_{iso} = -2515$, $\Omega = 1826$ and $\kappa = 0.90$) [71].

2.1.4. ^{195}Pt NMR

^{195}Pt, the only NMR-active isotope of platinum, has a high natural abundance (33.8%) and a moderate gyromagnetic ratio (5.8383×10^7 rad T^{-1} s^{-1}, corresponding to a spectral frequency of 85.92 MHz at 9.4 T). ^{195}Pt NMR has been employed to study a broad range of platinum-containing materials including catalytic systems [10,37,72,73], semi-conductors [74], and various platinum coordination complexes [43,75–79]. There is great variation in the magnitude of known platinum CSAs [80]: to date, the largest reported span obtained from ^{195}Pt SSNMR is that of K_2PtCl_4 ($\Omega = 10414$ ppm) [38]. We chose K_2PtCl_4 to test the effectiveness of WURST–CPMG for patterns beyond the observable bandwidth of a WURST experiment.

Fig. 4 depicts the ^{195}Pt NMR spectrum acquired with the WURST–CPMG pulse sequence. The pattern is too broad (*ca.* 980 kHz) to be collected in a single WURST–CPMG experiment; thus, piecewise acquisition is necessary. The collection of 5 sub-spectra at 400 kHz transmitter offsets was sufficient to obtain the entire powder pattern in just over 2 h (Table 1). Based on similar experiments on SnO, we estimate that using the CPMG sequence to obtain a ^{195}Pt NMR spectrum of similar quality would require at least 9 h (please refer to the Supporting Information for a full explanation of this estimate), as the reduced excitation bandwidth would necessitate the acquisition of more sub-spectra. Using an MAS experiment, Ellis et al. were able to acquire the total ^{195}Pt NMR spectrum in a piecewise fashion by collecting seven sub-spectra; [38] unfortunately, no experimental time is given for comparison. Not only does the WURST–CPMG experiment reduce the number of sub-spectra required to obtain the total powder pattern, it also provides a manifold of echo spikelets from which the platinum CS tensor can be accurately extracted, and avoids spectral artifacts from magic-angle mis-sets, resulting in a better overall powder pattern shape with a higher S/N. As with the previously discussed spectra, an echo spectrum resulting from the FT of spin-echoes coadded in the time domain was used for simulation purposes. The spans are in good agreement with previously published results, though the values of δ_{iso} are quite different, and the skews are fixed at -1.0 due to the D_{4h} symmetry of the $PtCl_4^{2-}$ anion [38].

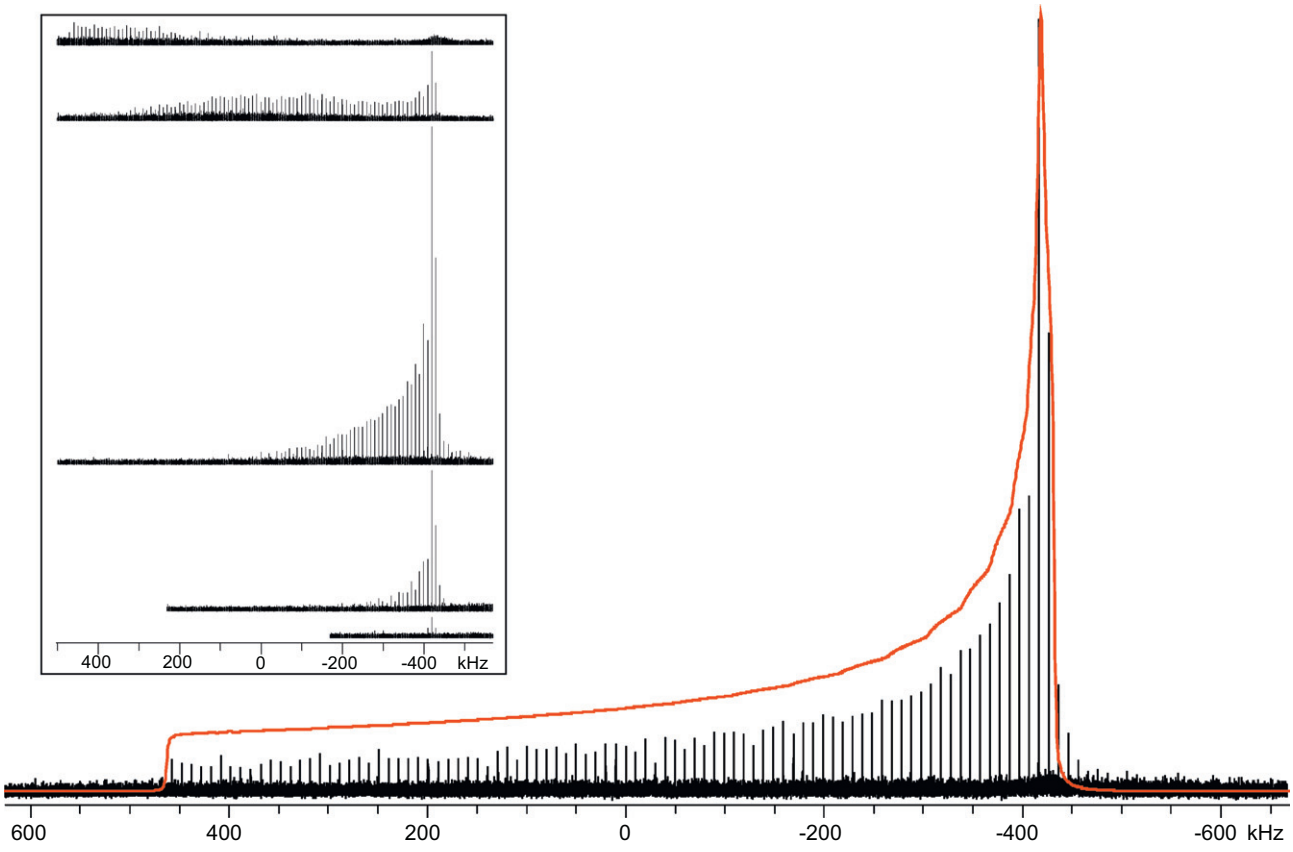

Fig. 4. ^{195}Pt WURST–CPMG NMR spectrum of K_2PtCl_4. The spectrum was acquired in a piecewise manner and is the sum of five sub-spectra, each of which consists of 40 transients. Inset: The five sub-spectra obtained during the piecewise acquisition.

2.2. ^{119}Sn UW SSNMR using pulses designed with optimal control theory

Broadband excitation pulses generated using OCT thus far have been designed for high-resolution solution NMR experiments. BEBOP and BIBOP [30–32] pulses have been developed which can uniformly excite or invert spin magnetization over the full ^{13}C chemical shift range at moderate B_1 field strengths (*ca.* 50 kHz). Constant-amplitude "calibration-free" pulses have also been reported [81], as well as ICEBERG pulses that result in transverse magnetization with a constant phase dispersion as a function of offset frequency [82]. There are also studies describing the use of OCT to optimize pulses for quadrupolar nuclei in applications to solids [33] and imaging [83,84]. As a preliminary investigation of the potential of optimized pulses for the acquisition of UW SSNMR spectra of spin-1/2 nuclei, we employed the open-source NMR simulation program SIMPSON to attempt to generate pulses capable of exciting the full width of the ^{119}Sn SSNMR spectrum of SnO at 9.4 T (*ca.* 150 kHz). In this case, the pulses are optimized to maximize the transverse magnetization for all crystallite orientations, which is associated with the I_{1x} detection operator in SIMPSON.

A variety of pulses were generated with different restrictions placed on their lengths and maximum RF amplitudes. We focus the discussion on the three best-performing pulses (Fig. 5), each of which is 50 μs in length and restricted to maximum RF powers of 15, 50 and 150 kHz (hereafter referred to as pulses A, B and C, respectively). Other pulse lengths (25 and 100 μs) were also tested; however, the 50 μs pulses were found to yield the best experimental lineshapes. The RF amplitude profiles of these optimized pulses resemble trains of "Gaussian-like" shapes which generally increase in amplitude with time, though, for the pulse limited to 15 kHz RF power, this "Gaussian-train" shape is severely truncated. This motif was observed in all of the pulses generated for this application. It is of interest to note that these pulse shapes closely resemble the polychromatic pulses published by Kupče and Freeman in 1994 [85], which were employed for broadband excitation of ^{13}C and ^{1}H solution NMR spectra. Kobzar et al. also observed similar shapes in a previous report on pulses generated with OCT [86]. The phase modulations of the pulses reported here are similar in each case: the phase is swept smoothly and relatively slowly through a range of *ca.* 10–50° over the course of each Gaussian-like amplitude modulation, but undergoes rapid jumps of 90–180° between each modulation.

Fig. 6A shows the ^{119}Sn pattern acquired from SnO using pulse A, and experimental and numerically simulated spectra obtained with a 15 kHz rectangular, monochromatic $\pi/2$ pulses for comparison. In each case the transmitter frequency was applied near the center of gravity of the pattern (−167 ppm). Pulse A results in a spectrum with all discontinuities clearly visible, and a more uniform excitation profile than that of the lineshape predicted by SIMPSON 2.0. The 15 kHz square pulse produces a spectrum that is clearly inferior, with only one clearly resolved discontinuity, and a signal intensity that drops significantly with increasing distance from the isotropic shift, as would be expected given its limited bandwidth. Fig. 6B compares the ^{119}Sn NMR spectra acquired with pulse B and a 50 kHz rectangular $\pi/2$ pulse. The 50 kHz rectangular pulse shows an improved performance over the 15 kHz rectangular pulse, as it is capable of exciting the full width of the spectrum such that all three discontinuities are resolved, although a drop in intensity is observed at the low frequency end of the pattern. The spectrum acquired with pulse B has a slightly rounded shoulder on the low frequency side, implying that either its excitation bandwidth is not quite as wide as the pattern, or that magnetization vectors corresponding to different orientations in different regions of the powder patterns are nutating at variable rates, similar to nutation phenomena in central-transition spectra of half-integer quadrupoles (a full numerical treatment is beyond the scope of this work) [87–89]. Both spectra are reasonable

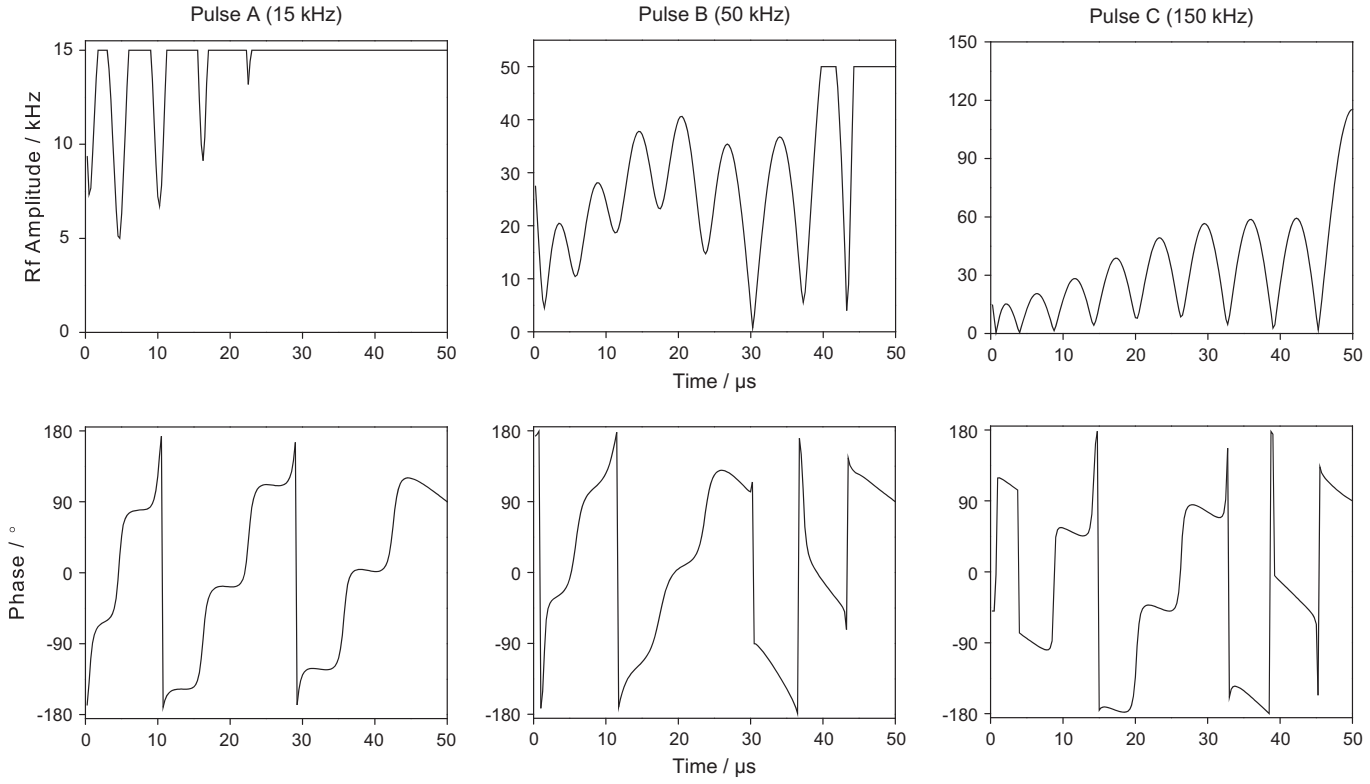

Fig. 5. RF amplitude and phase modulations for the ^{119}Sn excitation pulses used in this work, generated using the known parameters for SnO.

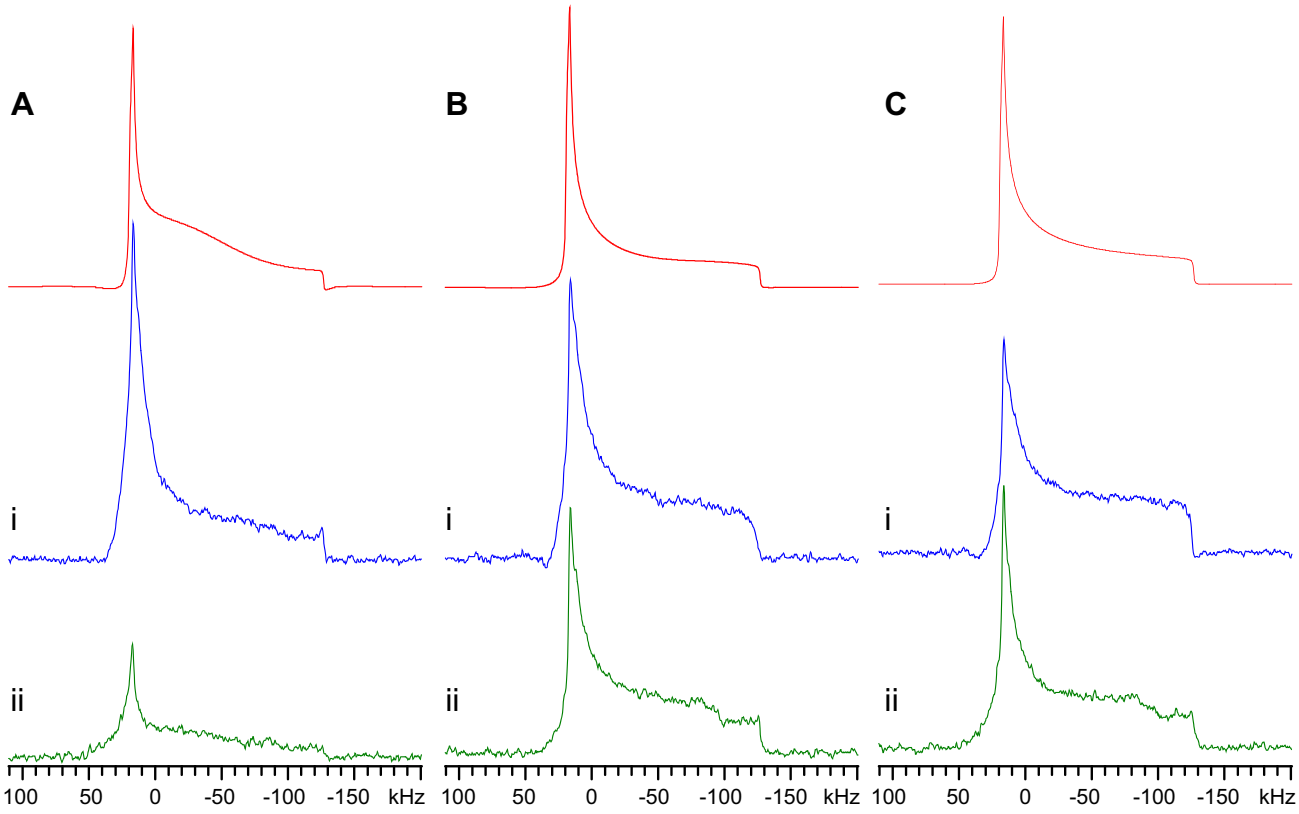

Fig. 6. ^{119}Sn NMR spectra of SnO acquired with an OCT pulse with (Ai) a 15 kHz maximum RF field, (Aii) a 15 kHz rectangular pulse, (Bi) an OCT pulse with a 50 kHz maximum RF field, (Bii) a 50 kHz rectangular pulse, (Ci) an OCT pulse with a 150 kHz maximum RF field and (Cii) a 150 kHz rectangular pulse. SIMPSON simulations of powder patterns resulting from a square pulse at each respective pulse strength are shown above the experimental spectra.

representations of the simulated powder pattern, though the spectrum acquired using pulse B more closely resembles the lineshape predicted by SIMPSON. Fig. 6C depicts the ^{119}Sn NMR spectrum of SnO acquired using pulse C, which was generated with a maximum permitted RF field of 150 kHz. In this case the maximum RF amplitude calculated by the OCT optimization is *ca.* 115 kHz, well below the maximum permitted value; hence, for comparison, a spectrum was obtained using a 115 kHz rectangular $\pi/2$ pulse. The spectrum acquired with pulse C is disproportionately intense on the low frequency end when compared to the lineshape predicted by SIMPSON 2.0, whereas the 115 kHz rectangular pulse produces a spectrum that matches the simulated lineshape reasonably well (though high-frequency discontinuity is still less intense than the idealized simulated lineshape).

Table 3 gives selected experimental details for the OCT experiments. Of the OCT pulses, pulses A and B yield spectra with similar S/N values (70 and 71, respectively), while the spectrum resulting from pulse C has a somewhat lower S/N (58). Of the standard rectangular pulses, the 15 kHz pulse has the worst S/N (27), while the 50 kHz and 115 kHz pulses has S/N values of 54 and 51, respectively. Hence, the performance of the OC and square pulses at the higher RF powers is comparable, but when the RF power is restricted, the OC pulses become advantageous. We also note that the WURST–CPMG (and CPMG) experiments produced spectra with nearly half the S/N of the best OCT and rectangular pulse experiments, despite being acquired with only one tenth the number of scans. In large part, this is due to the signal enhancement from acquiring many echoes with a train of refocusing pulses in the CPMG-type experiments. In cases where T_2 relaxation constants are very small (*i.e.*, where the CPMG-type experiments are not useful), pulses generated with OCT offer a useful, low-power alternative.

These preliminary results indicate that broadband excitation pulses optimized using OCT for the acquisition of broad CSA patterns are particularly advantageous at low RF powers, and therefore should be suitable for studying low-γ spin-1/2 nuclides such as ^{15}N, ^{57}Fe, ^{89}Y, ^{103}Rh and $^{107/109}$Ag, samples sensitive to RF heating, or in solid-state NMR studies of biological samples where high concentrations of ionic salts are present which can result in arcing within the probe. When high RF powers can be employed, these pulses would seem to offer little or no advantage over regular $\pi/2$ pulses in terms of excitation, at least over a range of up to *ca.* 150 kHz (we have yet to test this approach over greater frequency ranges). However, of all six spectra presented in this section, the spectrum acquired with pulse A most closely resembles the powder pattern predicted by SIMPSON 2.0. Hence, in terms of lineshape accuracy, the use of such optimized pulses may be advantageous (this was also noted in a study of excitation pulses generated for

Table 3
Comparison of selected ^{119}Sn SSNMR spectral parameters.

	S/N[a]	Experimental time (min.)	Number of scans
15 kHz OCT pulse	24.0	26.7	800
15 kHz rectangular pulse	10.7	26.7	800
50 kHz OCT pulse	18.0	26.7	800
50 kHz rectangular pulse	18.0	26.7	800
115 kHz OCT pulse	18.0	26.7	800
115 kHz rectangular pulse	19.0	26.7	800
30 kHz WURST–CPMG	24.0	2.7	80
75 kHz CPMG (piecewise)	22.3	26.7	80

[a] S/N ratios reported in this table are the average of S/N of points at δ_{11}, δ_{33} and δ_{iso} (see Table S5 for full listing). For CPMG-type experiments, the most intense spikelets nearest to these positions were used for S/N determination.

half-integer quadrupoles using OCT) [33]. Finally, we note that in order to take advantage of the significant signal enhancement available from the CPMG protocol, this approach will require the optimization of broadband refocusing pulses, which is not straightforward [29]. We are currently making preliminary investigations of such refocusing pulses.

3. Experimental

All solid-state NMR experiments were carried out on a Varian Infinity Plus NMR spectrometer, equipped with an Oxford 9.4 T ($\nu_0(^1H)$ = 400 MHz) wide-bore magnet operating at $\nu_0(^{207}Pb)$ = 83.50 MHz, $\nu_0(^{195}Pt)$ = 85.76 MHz, $\nu_0(^{199}Hg)$ = 71.39 MHz and $\nu_0(^{119}Sn)$ = 149.29 MHz. All experiments were performed on a Varian/Chemagnetics 4 mm HXY triple resonance probe, with samples tightly packed into 4 mm (o.d.) zirconium oxide rotors. SnO was purchased from Strem Chemicals, and all other samples [$Pb(OAc)_2{\cdot}3H_2O$ (where OAc = CH_3CHOO), $Hg(OAc)_2$, and K_2PtCl_4] were purchased from Sigma–Aldrich. The $Pb(OAc)_2{\cdot}3H_2O$ was recrystallized from aqueous solution, and the remaining samples were used without further purification.

^{207}Pb NMR chemical shifts are reported with respect to tetramethyl lead ($Pb(CH_3)_4$, δ_{iso} = 0.0 ppm) by using an aqueous solution of 0.5 M lead acetate hydrate ($Pb(CH_3COO)_2{\cdot}3H_2O$) as a secondary standard with an isotropic chemical shift of −2941 ppm [57]. ^{195}Pt chemical shifts are referenced with respect to 1.0 M Na_2PtCl_6 (aq) (δ_{iso} = 0.0 ppm) [77]. ^{199}Hg chemical shifts are reported with respect to $Hg(CH_3)_2$ by setting the isotropic shift of a saturated aqueous solution of $Hg(ClO_4)_2$ to −2253 ppm [90]. Finally, tetramethyltin ($Sn(CH_3)_4$) was used as a reference standard for ^{119}Sn NMR experiments, with its isotropic shift set to 0.0 ppm [91].

WURST–CPMG experiments employed recycle delays of 2, 7, 40 and 1450 s for the acquisition of all ^{119}Sn, ^{207}Pb, ^{195}Pt and ^{199}Hg NMR spectra, respectively. 50 μs pulse widths, and WURST-80 pulse shapes, were used for all WURST–CPMG experiments, with nutation frequencies of *ca.* 30, 67, 46 and 28 kHz for ^{119}Sn, ^{195}Pt, ^{207}Pb and ^{199}Hg, respectively. Between 64 and 250 Meiboom–Gill loops were acquired for the WURST–CPMG experiments, with an echo size of 200 points, and sweep range of 2 MHz in all cases. Further experimental details regarding the WURST–CPMG experiments can be found in the Supporting Information (Table S1).

The CPMG pulse sequence was used to acquire the ^{119}Sn SSNMR spectrum of SnO. 10 sub-spectra were acquired by stepping the transmitter frequency at 45 kHz intervals, then Fourier transformed and coadded to yield the complete powder pattern. A 3.33 μs 90° pulse was employed, corresponding to an RF field of *ca.* 75 kHz. 64 Meiboom–Gill loops of 200 points were acquired for each transient, with a 2.0 s recycle delay. Further experimental details are summarized in Table S2.

The CP–CPMG sequence [45,46] was employed to obtain the ^{207}Pb NMR spectrum of $Pb(CH_3OO)_2{\cdot}3H_2O$. 9 echoes were acquired in a piecewise manner at 20 kHz offsets, then coadded after being Fourier transformed to yield the complete spectrum. A Hartmann–Hahn matching condition of $\nu_{CP}(^1H) = \nu_{CP}(^{207}Pb) \approx 48$ kHz was used. 80 Meiboom–Gill loops were acquired per scan, each of which was 200 points in length, and a 4.0 s pulse delay was employed between scans. Further experimental details regarding the CP–CPMG experiment can be found in Table S3.

The TPPM decoupling scheme [92] was employed for the acquisition of ^{207}Pb and ^{199}Hg CP–CPMG and CPMG NMR spectra, respectively, whereas CW decoupling was employed in all WURST–CPMG experiments. Tests of CW and TPPM decoupling for both ^{199}Hg and ^{207}Pb CPMG and WURST–CPMG experiments produced no discernable difference in S/N, experiment times, etc. We also note that in previous work by our group, we observed no noticeable difference in performance between CW and TPPM decoupling methods when recording UW spectra from static samples; therefore, choice of decoupling method should have no bearing on comparison of spectra acquired with different experiments [93]. Unless otherwise indicated, analytical simulations of static SSNMR spectra for the extraction of CS tensor parameters are based upon spectra produced from the time domain coaddition of spin-echoes from WURST–CPMG experiments. This involves summing the spin-echoes in the time domain, which produces an FID resembling that of a standard echo sequence. This coadded echo is Fourier transformed, and a magnitude calculation is applied to obtain a spectrum of standard appearance (rather than spikelets), which has an outer manifold that is more easily simulated. WURST–CPMG spectra processed in this way can be found in the Supporting Information (Fig. S2), or in the case of $Hg(OAc)_2$, in Fig. 3. Numerical simulations of WURST–CPMG powder patterns were also carried out using SIMPSON [28,29] to verify and refine the simulated parameter values. Additional simulations of experimental spectra from CPMG and CP–CPMG experiments were also carried out using the WSolids simulation package [94] and/or DMFit [95] simulation software.

Optimized pulses employed during OCT experiments were generated using SIMPSON (ver. 2.0) [29] on a desktop computer with the Windows XP operating system. SnO was chosen as a test sample for all OCT experiments due to the receptive nature of the ^{119}Sn nucleus and its well known CS tensor parameters [40]. The CS tensor parameters used for the generation of all optimized pulses were Ω = 976 ppm and κ = 0.96, which are based on a simulation of a ^{119}Sn SSNMR spectrum acquired previously using the WURST–CPMG sequence. 376 crystallite orientations were used to optimize each pulse, and 28,656 crystallite orientations were used to produce corresponding numerical simulations. These orientations were calculated using the ZCW method [96–98]. Each pulse generated using OCT was composed of 200 elements of length 0.25 μs, with constant amplitude and phase during each of the constituent elements. The optimized pulses resulted from the optimization of initial, random pulse shapes, with the RF field limited by a maximum value. The pulse shapes were output as text files and manually converted into the P-code format required for use with the Varian Spinsight software. Simulations of all spectra related to the OCT portion of this work were carried out using SIMPSON (ver. 2.0) [28,29]. All spectra were processed using NUTS (Acorn NMR).

4. Conclusions

The WURST–CPMG pulse sequence has successfully been applied in the acquisition of wideline and UW SSNMR patterns of various spin-1/2 nuclides. In comparison to the CPMG sequence, WURST–CPMG offers a significant reduction in experimental time in the acquisition of the ^{119}Sn SSNMR spectrum of SnO, removing the need for piecewise acquisition. Similarly, ^{207}Pb WURST–CPMG NMR proves to be more efficient than the ^{1}H–^{207}Pb CP–CPMG sequence in acquiring the ^{207}Pb SSNMR spectrum of $Pb(OAc)_2{\cdot}3H_2O$, as the entire pattern could be acquired in a single experiment, and in a shorter period of time. In cases where the T_1 of the X nucleus is very long compared to the $T_1(^1H)$ (*e.g.,* for ^{199}Hg SSNMR experiments on $Hg(OAc)_2$), CP–CPMG may prove to be more efficient; however, CP is not always feasible (*i.e.,* ^{1}H or ^{19}F are not present in the sample), in which case WURST–CPMG is an extremely useful alternative. For SSNMR spectra that exceed the excitation bandwidth of WURST–CPMG pulses (*e.g.,* ^{195}Pt NMR of K_2PtCl_4), piecewise acquisition can be readily employed to obtain the total powder pattern.

Preliminary experiments making use of pulses generated with OCT indicate that low-power pulses can be created which outper-

form standard, rectangular pulses of the same power for the acquisition of broad spin-1/2 SSNMR patterns. The improvements in signal intensity and powder pattern shape provided by OCT pulses at low-power levels are reduced as the pulse power is increased, though for samples sensitive to increases in temperature, samples containing low-γ nuclei or solution samples with high salt concentrations, these pulses may be a useful alternative to standard rectangular pulses. For the acquisition of the ^{119}Sn SSNMR spectrum of SnO, WURST–CPMG is the best method of acquisition; however, in cases where T_2 relaxation constants are very small, pulses generated using OCT offer a reasonable alternative.

We hope that this article encourages further investigations of the broad powder patterns of heavy spin-1/2 nuclides, since their acute sensitivity to the surrounding electronic structure could greatly enhance our understanding of structure and dynamics for a broad array of materials. These techniques will be very useful for further NMR investigations of a number of additional spin-1/2 nuclei which may have broad patterns arising from CSA or disorder at the atomic/molecular level, including metal nuclides like ^{77}Se, ^{29}Si, ^{125}Te, ^{181}Yb, and of course low-gamma nuclides such as ^{15}N, ^{57}Fe, ^{89}Y, ^{103}Rh and $^{107/109}$Ag.

Acknowledgments

We thank the Natural Sciences and Engineering Research Council (NSERC, Canada), the Canadian Foundation for Innovation, the Ontario Innovation Trust and the University of Windsor for funding the solid-state NMR facility at the University of Windsor. A.W.M. is grateful for a graduate tuition scholarship provided by the University of Windsor. R.W.S. thanks the Ontario Ministry of Research and Innovation for an Early Researcher Award, and the Centre for Catalysis and Materials Research at the University of Windsor for providing additional funding. Dr. Stephen J. Loeb at the University of Windsor is also thanked for providing the K_2PtCl_4 sample.

Appendix A. Supplementary material

Supplementary data associated with this article can be found, in the online version, at doi:10.1016/j.jmr.2010.10.011.

References

[1] G. Neue, C. Dybowski, M.L. Smith, D.H. Barich, Solid State Nucl. Magn. Reson. 3 (1994) 115–119.
[2] J.A. Tang, L.A. O'Dell, P.M. Aguiar, B.E.G. Lucier, D. Sakellariou, R.W. Schurko, Chem. Phys. Lett. 466 (2008) 227–234.
[3] P.L. Bryant, C.R. Harwell, A.A. Mrse, E.F. Emery, Z.H. Gan, T. Caldwell, A.P. Reyes, P. Kuhns, D.W. Hoyt, L.S. Simeral, R.W. Hall, L.G. Butler, J. Am. Chem. Soc. 123 (2001) 12009–12017.
[4] A.S. Lipton, G.W. Buchko, J.A. Sears, M.A. Kennedy, P.D. Ellis, J. Am. Chem. Soc. 123 (2001) 992–993.
[5] H. Hamaed, A.Y.H. Lo, D.S. Lee, W.J. Evans, R.W. Schurko, J. Am. Chem. Soc. 128 (2006) 12638–12639.
[6] M.A.M. Forgeron, R.E. Wasylishen, Magn. Reson. Chem. 46 (2008) 206–214.
[7] P. Crewdson, D.L. Bryce, F. Rominger, P. Hofmann, Angew. Chem. – Int. Edit. 47 (2008) 3454–3457.
[8] V.K. Michaelis, P.M. Aguiar, V.V. Terskikh, S. Kroeker, Chem. Commun. (2009) 4660–4662.
[9] A.J. Rossini, R.W. Mills, G.A. Briscoe, E.L. Norton, S.J. Geier, I. Hung, S. Zheng, J. Autschbach, R.W. Schurko, J. Am. Chem. Soc. 131 (2009) 3317–3330.
[10] H.E. Rhodes, P.K. Wang, H.T. Stokes, C.P. Slichter, J.H. Sinfelt, Phys. Rev. B 26 (1982) 3559–3568.
[11] T.J. Bastow, M.E. Smith, Solid State Nucl. Magn. Reson. 1 (1992) 165–174.
[12] E.V. Sampathkumaran, N. Fujiwara, S. Rayaprol, P.K. Madhu, Y. Uwatoko, Phys. Rev. B (2004) 70.
[13] D. Massiot, I. Farnan, N. Gautier, D. Trumeau, A. Trokiner, J.P. Coutures, Solid State Nucl. Magn. Reson. 4 (1995) 241–248.
[14] A. Medek, V. Frydman, L. Frydman, J. Phys. Chem. A 103 (1999) 4830–4835.
[15] A.S. Lipton, T.A. Wright, M.K. Bowman, D.L. Reger, P.D. Ellis, J. Am. Chem. Soc. 124 (2002) 5850–5860.
[16] F.H. Larsen, H.J. Jakobsen, P.D. Ellis, N.C. Nielsen, J. Phys. Chem. A 101 (1997) 8597–8606.
[17] A.S. Lipton, J.A. Sears, P.D. Ellis, J. Magn. Reson. 151 (2001) 48–59.
[18] I. Hung, R.W. Schurko, J. Phys. Chem. B 108 (2004) 9060–9069.
[19] J.A. Tang, J.D. Masuda, T.J. Boyle, R.W. Schurko, ChemPhysChem 7 (2006) 117–130.
[20] J.A. Tang, B.D. Ellis, T.H. Warren, J.V. Hanna, C.L.B. Macdonald, R.W. Schurko, J. Am. Chem. Soc. 129 (2007) 13049–13065.
[21] A.S. Lipton, R.W. Heck, S. Primak, D.R. McNeill, D.M. Wilson, P.D. Ellis, J. Am. Chem. Soc. 130 (2008) 9332–9341.
[22] L.A. O'Dell, R.W. Schurko, Chem. Phys. Lett. 464 (2008) 97–102.
[23] K. Yamauchi, J.W.G. Janssen, A.P.M. Kentgens, J. Magn. Reson. 167 (2004) 87–96.
[24] A.P.M. Kentgens, J. Bart, P.J.M. van Bentum, A. Brinkmann, E.R.H. Van Eck, J.G.E. Gardeniers, J.W.G. Janssen, P. Knijn, S. Vasa, M.H.W. Verkuijlen, J. Chem. Phys. (2008) 128.
[25] R. Bhattacharyya, L. Frydman, J. Chem. Phys. (2007) 127.
[26] E. Kupce, R. Freeman, J. Magn. Reson. Ser. A 115 (1995) 273–276.
[27] L.A. O'Dell, A.J. Rossini, R.W. Schurko, Chem. Phys. Lett. 468 (2009) 330–335.
[28] M. Bak, J.T. Rasmussen, N.C. Nielsen, J. Magn. Reson. 147 (2000) 296–330.
[29] Z. Tosner, T. Vosegaard, C. Kehlet, N. Khaneja, S.J. Glaser, N.C. Nielsen, J. Magn. Reson. 197 (2009) 120–134.
[30] T.E. Skinner, T.O. Reiss, B. Luy, N. Khaneja, S.J. Glaser, J. Magn. Reson. 163 (2003) 8–15.
[31] T.E. Skinner, T.O. Reiss, B. Luy, N. Khaneja, S.J. Glaser, J. Magn. Reson. 167 (2004) 68–74.
[32] K. Kobzar, T.E. Skinner, N. Khaneja, S.J. Glaser, B. Luy, J. Magn. Reson. 170 (2004) 236–243.
[33] L.A. O'Dell, K.J. Harris, R.W. Schurko, J. Magn. Reson. 203 (2010) 156–166.
[34] R. Siegel, T.T. Nakashima, R.E. Wasylishen, Concepts Magn. Reson. Part A 26A (2005) 47–61.
[35] G.M. Bowers, A.S. Lipton, K.T. Mueller, Solid State Nucl. Magn. Reson. 29 (2006) 95–103.
[36] H. Hamaed, M.W. Laschuk, V.V. Terskikh, R.W. Schurko, J. Am. Chem. Soc. 131 (2009) 8271–8279.
[37] C.D. Makowka, C.P. Slichter, J.H. Sinfelt, Phys. Rev. B 31 (1985) 5663–5679.
[38] S.W. Sparks, P.D. Ellis, J. Am. Chem. Soc. 108 (1986) 3215–3218.
[39] C.P. Grey, C.M. Dobson, A.K. Cheetham, R.J.B. Jakeman, J. Am. Chem. Soc. 111 (1989) 505–511.
[40] C. Cossement, J. Darville, J.M. Gilles, J.B. Nagy, C. Fernandez, J.P. Amoureux, Magn. Reson. Chem. 30 (1992) 263–270.
[41] G.A. Bowmaker, R.K. Harris, S.W. Oh, Coord. Chem. Rev. 167 (1997) 49–94.
[42] G.G. Briand, A.D. Smith, G. Schatte, A.J. Rossini, R.W. Schurko, Inorg. Chem. 46 (2007) 8625–8637.
[43] J.A. Tang, E. Kogut, D. Norton, A.J. Lough, B.R. McGarvey, U. Fekl, R.W. Schurko, J. Phys. Chem. B 113 (2009) 3298–3313.
[44] R.A. Santos, E.S. Gruff, S.A. Koch, G.S. Harbison, J. Am. Chem. Soc. 113 (1991) 469–475.
[45] I. Hung, A.J. Rossini, R.W. Schurko, J. Phys. Chem. A 108 (2004) 7112–7120.
[46] R. Siegel, T.T. Nakashima, R.E. Wasylishen, J. Phys. Chem. B 108 (2004) 2218–2226.
[47] E.M. Menger, D.P. Raleigh, R.G. Griffin, J. Magn. Reson. 63 (1985) 579–582.
[48] C. Groombridge, J. Magn. Reson. Chem. 31 (1993) 380–387.
[49] A.K. Cheetham, C.M. Dobson, C.P. Grey, R.J.B. Jakeman, Nature 328 (1987) 706–707.
[50] N.J. Clayden, C.M. Dobson, A. Fern, J. Chem. Soc. – Dalton Trans. (1989) 843–847.
[51] S. de Monredon, A. Cellot, F. Ribot, C. Sanchez, L. Armelao, L. Gueneau, L. Delattre, J. Mater. Chem. 12 (2002) 2396–2400.
[52] L.A. O'Dell, S.L.P. Savin, A.V. Chadwick, M.E. Smith, Nanotechnology 16 (2005) 1836–1843.
[53] V. Sepelak, K.D. Becker, I. Bergmann, S. Suzuki, S. Indris, A. Feldhoff, P. Heitjans, C.P. Grey, Chem. Mater. 21 (2009) 2518–2524.
[54] R.K. Harris, A. Sebald, D. Furlani, G. Tagliavini, Organometallics 7 (1988) 388–394.
[55] D.C. Apperley, N.A. Davies, R.K. Harris, A.K. Brimah, S. Eller, R.D. Fischer, Organometallics 9 (1990) 2672–2676.
[56] H.P. Bai, R.K. Harris, H. Reuter, J. Organomet. Chem. 408 (1991) 167–172.
[57] F. Fayon, I. Farnan, C. Bessada, J. Coutures, D. Massiot, J.P. Coutures, J. Am. Chem. Soc. 119 (1997) 6837–6843.
[58] P.D. Zhao, S. Prasad, J. Huang, J.J. Fitzgerald, J.S. Shore, J. Phys. Chem. B 103 (1999) 10617–10626.
[59] J.B. Grutzner, K.W. Stewart, R.E. Wasylishen, M.D. Lumsden, C. Dybowski, P.A. Beckmann, J. Am. Chem. Soc. 123 (2001) 7094–7100.
[60] S.E. Van Bramer, A. Glatfelter, S. Bai, C. Dybowski, G. Neue, D.L. Perry, Magn. Reson. Chem. 44 (2006) 357–365.
[61] C. Dybowski, G. Neue, Prog. Nucl. Magn. Reson. Spectrosc. 41 (2002) 153–170.
[62] L.C.M. Van Gorkom, J.M. Hook, M.B. Logan, J.V. Hanna, R.E. Wasylishen, Magn. Reson. Chem. 33 (1995) 791–795.
[63] A. Bielecki, D.P. Burum, J. Magn. Reson. Ser. A 116 (1995) 215–220.
[64] A.D. Irwin, C.D. Chandler, R. Assink, M. Hampdensmith, J. Inorg. Chem. 33 (1994) 1005–1006.
[65] Y.S. Kye, S. Connolly, B. Herreros, G.S. Harbison, Main Group Met. Chem. 22 (1999) 373–383.
[66] A.C. Larsson, A.V. Ivanov, K.J. Pike, W. Forsling, O.N. Antzutkin, J. Magn. Reson. 177 (2005) 56–66.
[67] L.M. Utschig, J.W. Bryson, T.V. Ohalloran, Science 268 (1995) 380–385.
[68] G.A. Bowmaker, R.K. Harris, D.C. Apperley, Inorg. Chem. 38 (1999) 4956–4962.

[69] R.J. Goodfellow, in: J. Mason (Ed.), Multinuclear NMR, 1st ed., Plenum Press, New York, 1987.
[70] R.K. Harris, A. Sebald, Magn. Reson. Chem. 25 (1987) 1058–1062.
[71] K. Eichele, S. Kroeker, G. Wu, R.E. Wasylishen, Solid State Nucl. Magn. Reson. 4 (1995) 295–300.
[72] Y.Y. Tong, C. Rice, A. Wieckowski, E. Oldfield, J. Am. Chem. Soc. 122 (2000) 11921–11924.
[73] Y.Y. Tong, A. Wieckowski, E. Oldfield, J. Phys. Chem. B 106 (2002) 2434–2446.
[74] A. Grykalowska, B. Nowak, Solid State Nucl. Magn. Reson. 27 (2005) 223–227.
[75] D.M. Doddrell, P.F. Barron, D.E. Clegg, C. Bowie, J. Chem. Soc.-Chem. Commun. (1982) 575–576.
[76] J.J. Dechter, J. Kowalewski, J. Magn. Reson. 59 (1984) 146–149.
[77] R.K. Harris, P. Reams, K.J. Packer, J. Chem. Soc.-Dalton Trans. (1986) 1015–1020.
[78] R.K. Harris, I.J. McNaught, P. Reams, K. Packer, J. Magn. Reson. Chem. 29 (1991) S60–S72.
[79] E.J.W. Austin, P.J. Barrie, R.J.H. Clark, J. Chem. Soc.-Chem. Commun. (1993) 1404–1405.
[80] R.J. Goodfellow (Ed.), Group VIII Transition Metals, 1st ed., Plenum Press, New York, 1987.
[81] T.E. Skinner, K. Kobzar, B. Luy, M.R. Bendall, W. Bermel, N. Khaneja, S.J. Glaser, J. Magn. Reson. 179 (2006) 241–249.
[82] N.I. Gershenzon, T.E. Skinner, B. Brutscher, N. Khaneja, M. Nimbalkar, B. Luy, S.J. Glaser, J. Magn. Reson. 192 (2008) 235–243.
[83] J.S. Lee, R.R. Regatte, A. Jerschow, J. Chem. Phys. (2008) 129.
[84] J.S. Lee, R.R. Regatte, A. Jerschow, J. Chem. Phys. (2009) 131.
[85] E. Kupce, R. Freeman, J. Magn. Reson. Ser. A 108 (1994) 268–273.
[86] K. Kobzar, T.E. Skinner, N. Khaneja, S.J. Glaser, B. Luy, J. Magn. Reson. 194 (2008) 58–66.
[87] A. Samoson, E. Kundla, E. Lippmaa, J. Magn. Reson. 49 (1982) 350–357.
[88] A. Samoson, E. Lippmaa, Chem. Phys. Lett. 100 (1983) 205–208.
[89] A. Samoson, E. Lippmaa, Phys. Rev. B 28 (1983) 6567–6570.
[90] J.M. Hook, P.A.W. Dean, L.C.M. Vangorkom, Magn. Reson. Chem. 33 (1995) 77–79.
[91] R.K. Harris, E.D. Becker, S.M.C. De Menezes, R. Goodfellow, P. Granger, Pure Appl. Chem. 73 (2001) 1795–1818.
[92] A.E. Bennett, C.M. Rienstra, M. Auger, K.V. Lakshmi, R.G. Griffin, J. Chem. Phys. 103 (1995) 6951–6958.
[93] L.A. O'Dell, R.W. Schurko, Phys. Chem. Chem. Phys. 11 (2009) 7069–7077.
[94] K. Eichele, R.E. Wasylishen, WSolids: Solid-State NMR Spectrum Simul. (2001).
[95] D. Massiot, F. Fayon, M. Capron, I. King, S. Le Calve, B. Alonso, J.O. Durand, B. Bujoli, Z.H. Gan, G. Hoatson, Magn. Reson. Chem. 40 (2002) 70–76.
[96] S. Zaremba, Ann. Mat. Pura. Appl. 73 (1966) 293–317.
[97] H. Conroy, J. Chem. Phys. 47 (1967) 5307.
[98] V.B. Cheng, H.H. Suzukawa, M. Wolfsber, J. Chem. Phys. 59 (1973) 3992–3999.